Journal of Engineering Mathematics **27**: 419–432, 1993.

Fully non-linear two-layer flow over arbitrary topography

S.R. BELWARD[1] and L.K. FORBES

Centre for Industrial and Applied Mathematics and Parallel Computing, Department of Mathematics, The University of Queensland, Queensland, 4072, Australia

Received 9 June 1992; accepted in revised form 20 April 1993

Abstract. Steady, two-dimensional, two-layer flow over an arbitrary topography is considered. The fluid in each layer is assumed to be inviscid and incompressible and flows irrotationally. The interfacial surface is found using a boundary integral formulation, and the resulting integrodifferential equations are solved iteratively using Newton's method. A linear theory is presented for a given topography and the non-linear theory is compared against this to show how the non-linearity affects the problem.

1. Introduction

The problem of free surface fluid flow over obstacles has a long and well documented history. The many variations this problem can take have been used to model situations in engineering and the atmospheric and oceanographic sciences.

The simplest form the problem can take is when the flow consists of a single layer of inviscid, incompressible fluid flowing over an obstacle. Kelvin [1] presented a linear theory for the steady form of this problem. Much work since then has involved the use of submerged singularities to describe flow over obstacles. Wehausen and Laitone [2] provide a good review of the literature on this subject.

More recently, boundary element methods have been used to solve the exact non-linear problem. However, in most cases, the specific geometry involved in the problem has been used to simplify the equations. Arbitrary bottom profiles are thus not generally permitted. For example, Forbes [3] and [4] considered flow of a single fluid layer over a semi-elliptical obstacle on the stream bed, and used conformal mapping to satisfy the bottom condition exactly. Forbes and Schwartz [5] considered flow over a semi-circular obstruction and Dias and Vanden-Broeck [6] studied the flow over a triangular weir. An exception is the work of King and Bloor [7] who in fact allowed an arbitrary bottom topography and a single layer of inviscid, incompressible fluid. A generalisation of the Schwarz–Christoffel transformation was used and the resulting integral and integrodifferential equations were solved numerically. We present a simpler approach and extend it to the case of two fluid layers, so that the single layer problem is the special case when the upper layer has zero weight. Also popular recently are asymptotic theories of fluid flow in channels. For example, Grimshaw and Smyth [8] solved a forced Korteweg-de Vries equation describing weakly non-linear resonant flow of

[1] Current address: Department of Mathematics and Statistics, James Cook University of North Queensland, Townsville, Queensland, 4811, Australia.

a stratified fluid over an obstacle, and Shen [9] investigated the problem of near critical flow in a channel with an inviscid fluid of constant density using a similar forced Korteweg-de Vries equation.

In considering the problem of flow over obstacles in a meteorological or oceanographic situation, a single layer approximation becomes insufficient, as the fluid is now continuously stratified. The next step in modelling an atmospheric situation could well be considered to be a two-layer system of fluid where the fluid in each layer is inviscid and incompressible. One could envisage this configuration to occur in the atmosphere when, for example, a mass of cool relatively dense air is expelled underneath a mass of warm less dense air in the downdraft associated with a thunderstorm. This is the situation modelled in this paper.

Shen [10] considered a similar two-layer system, which was solved again using a forced Korteweg-de Vries equation to approximate the governing equations. However, the fully non-linear problem remains unsolved. An associated problem is that of interfacial waves between two inviscid fluids of constant density. In this case, the mechanism of generation of the wave is disregarded and the limiting periodic wave profile is sought. It is now known that this limiting profile is a mushroom-shaped structure as observed by Grimshaw and Pullin [11] and Turner and Vanden-Broeck [12]. Earlier, however, Holyer [13] had been only able to obtain a limiting wave profile with a vertical tangent; no overhang could be found, since this was not permitted in her numerical technique.

In Section 2 we formulate the problem as a system of three coupled integrodifferential equations. These equations govern the fully non-linear flow over arbitrary topography of two layers of inviscid, incompressible fluid. A linear solution is presented in Section 3, while in Section 4, the integrodifferential equations are discretised and solved iteratively, extending a technique used by Forbes [3]. Section 5 contains the results of our computational experiments where the governing parameters were varied. We also consider the drag produced by the obstacle. In Section 6, we present a summary and discuss further areas for research.

2. Formulation

We consider a system of two layers of constant density fluid, one on top of the other, flowing over arbitrary topography. The profile of the topography is given by $y = B(x)$ where x and y are horizontal and vertical coordinates, respectively. The upper fluid layer is bounded by a rigid lid. The flow is two-dimensional, irrotational and far upstream is uniform. We let subscript 1 refer to variables in the upper layer and subscript 2 refer to variables in the lower layer. We then denote the upstream depth of each layer by H_1 and H_2 and the upstream horizontal velocity in each layer by c_1 and c_2. Densities, velocities and pressures in each layer are ρ_j, $\mathbf{q}_j$ and p_j, $j = 1, 2$. The interface between the two fluids, which is unknown at the outset, is given by $y = S(x)$. Only waves that are stationary with respect to the mountain are considered, so partial derivatives with respect to time are taken to be zero. The fluid system is shown schematically in Fig. 1.

The variables above are non-dimensionalised using H_2 as the the length scale and c_2 as the velocity scale. The lower layer then has an upstream uniform speed of 1 and an upstream uniform height of 1. We define the four dimensionless parameters which describe properties of the flow,

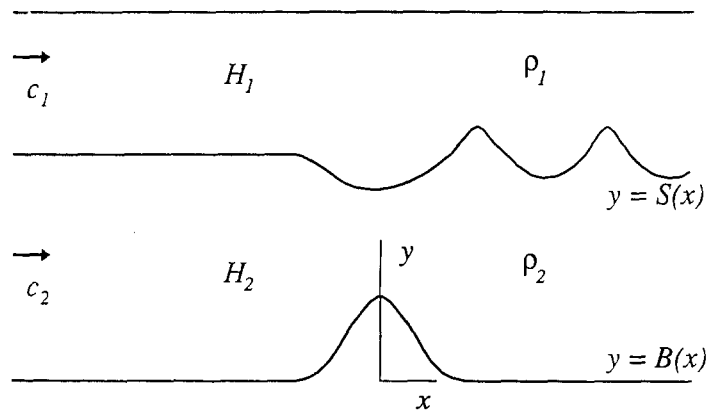

Fig. 1. Schematic diagram of the two layer fluid system flowing over an arbitrary obstacle $y = B(x)$. The unknown interface $y = S(x)$ is to be obtained, and once known, enables any other quantity in either fluid layer to calculated.

$$
\begin{aligned}
F_2 &= \frac{c_2}{\sqrt{gH_2}} && \text{the Froude number in the lower layer,} \\
\gamma &= \frac{c_1}{c_2} && \text{the ratio of upstream fluid speeds,} \\
D &= \frac{\rho_1}{\rho_2} && \text{the ratio of densities,} \\
\lambda &= \frac{H_1}{H_2} && \text{the ratio of upstream fluid heights,}
\end{aligned}
\tag{2.1}
$$

and two dimensionless parameters which describe properties of the obstacle, h the maximum obstacle height, and L the obstacle half length. The following work proceeds purely with non-dimensionalised variables.

Let ϕ_j, $j = 1, 2$ be the velocity potentials in each layer, so, $u_j = \partial\phi_j/\partial x$ and $v_j = \partial\phi_j/\partial y$ where u_j and v_j are, respectively, the horizontal and vertical components of the velocity vectors $\mathbf{q}_j$. Then within each fluid, the continuity equation yields

$$\nabla^2\phi_j = 0\,, \quad j = 1, 2\,, \tag{2.2}$$

and on the upper boundary, the condition of no penetration is

$$\nabla\phi_1 \cdot \mathbf{n} = 0 \quad \text{on} \quad y = \lambda + 1\,. \tag{2.3}$$

Similarly, at the interface $y = S(x)$, there is no fluid exchange and so

$$\nabla\phi_j \cdot \mathbf{n} = 0 \quad \text{for} \quad j = 1, 2 \quad \text{on} \quad y = S(x)\,. \tag{2.4}$$

Again for the bottom we have the no penetration condition

$$\nabla\phi_2 \cdot \mathbf{n} = 0 \quad \text{on} \quad y = B(x)\,. \tag{2.5}$$

At the fluid interface, continuity of pressure, coupled with the Bernoulli equation in each layer of fluid gives the interface condition

$$\frac{1}{2}F_2^2(q_2^2 - Dq_1^2) + (1-D)S(x) = \frac{1}{2}F_2^2(1 - D\gamma^2) + 1 - D \quad \text{on} \quad y = S(x)\,. \tag{2.6}$$

The upstream conditions are

$$\mathbf{q}_1 \to \gamma\mathbf{i}\,, \quad \mathbf{q}_2 \to \mathbf{i}\,, \quad S(x) \to 1 \quad \text{as} \quad x \to -\infty\,. \tag{2.7}$$

Equations (2.2)–(2.7) then are the equations to be solved.

We introduce the complex variable $z = x + \mathrm{i}y$, and then the complex velocity potential is $w_j = \phi_j + \mathrm{i}\psi_j$ where ψ_j, $j = 1, 2$ is the stream function in each layer. The w_j are analytic functions of z because ϕ_j and ψ_j satisfy the Cauchy–Riemann equations, since the fluid is incompressible and flows irrotationally. The conjugate complex velocity in each layer is given by $\mathrm{d}w_j/\mathrm{d}z = u_j - \mathrm{i}v_j$.

Previous studies on flow over specific topographies (for example, Dias and Vanden-Broeck [6] (triangular wier), Forbes [3] and [4] (semi-elliptical obstacle) and Forbes and Schwartz [5] (semi-circular obstacle)) have used an inverse formulation to enable a simpler representation of the free surface boundary conditions involved in each problem. Typically ϕ_j and ψ_j defined above would be chosen as the independent variables so that equation (2.6) would then be satisfied on the known location $\psi_2 = 1$ rather than the unknown $y = S(x)$. King and Bloor [7] also used an inverse technique to calculate flow over arbitrary topography. However, as noted in the Introduction, their formulation involved the use of a rather complicated Schwarz–Christoffel transformation.

To avoid such complication in presenting a method capable of obtaining solutions for arbitrary topography we use a direct method, in which the unknown interface is calculated using integrodifferential equations for the complex velocity on the boundaries and the interface of the fluid system. In formulating these equations an arclength, s, is used to parametrise the interface. This arclength must satisfy

$$\left(\frac{\mathrm{d}x}{\mathrm{d}s}\right)^2 + \left(\frac{\mathrm{d}y}{\mathrm{d}s}\right)^2 = 1\,. \tag{2.8}$$

The coordinates of the interface are then $(x,\ S(x)) = (x(s),\ y(s))$ and the velocity components on the interface are given by

$$u_j = \frac{\mathrm{d}x}{\mathrm{d}s}\frac{\mathrm{d}\phi_j}{\mathrm{d}s} \quad \text{and} \quad v_j = \frac{\mathrm{d}y}{\mathrm{d}s}\frac{\mathrm{d}\phi_j}{\mathrm{d}s}\,, \quad j = 1, 2$$

and Bernoulli's equation (2.6) on the interface becomes

$$\frac{1}{2}F_2^2\left[\left(\frac{\mathrm{d}\phi_2}{\mathrm{d}s}\right)^2 - D\left(\frac{\mathrm{d}\phi_1}{\mathrm{d}s}\right)^2\right] + (1-D)y(s) = \frac{1}{2}F_2^2(1 - D\gamma^2) + 1 - D\,. \tag{2.9}$$

The integrodifferential equations are obtained using Cauchy's integral formula. The first equation is derived by reflecting the upper layer (layer 1) about the horizontal top $y = \lambda + 1$ of the two fluid system. This produces an image fluid region, bounded by the reflection of the interface $y = S(x)$ in the line $y = \lambda + 1$. In this region equation (2.3) requires that the vertical velocity satisfy the reflection condition

$$v_1(x, y) = -v_1(x, 2\lambda + 2 - y)\,.$$

We apply Cauchy's integral formula to the complex function $\chi_1(z) = \mathrm{d}w_1/\mathrm{d}z - \gamma$ to give

$$\oint_\Gamma \frac{\chi_1(z)\,\mathrm{d}z}{z - z(s)} = 0\,. \tag{2.10}$$

Here the path Γ consists of the interfacial surface with a semi-circular path of vanishingly small radius excluding the point $z(s)$, the entire image surface and the vertical lines $x = \pm L$ with $L \to \infty$. The integration variable z represents any point on the contour Γ. In the limit $L \to \infty$, the contributions from the two vertical lines become zero. Let σ be the value of the arclength at the moveable point $z(\sigma)$ on the contour Γ; then from equation (2.10) we have

$$\begin{aligned} \mathrm{i}\pi\chi_1(Z(s) + \mathrm{i}(\lambda+1)) = &\int_{-\infty}^{\infty} \frac{\chi_1(Z(\sigma) + \mathrm{i}(\lambda+1))Z'(\sigma)\,\mathrm{d}\sigma}{Z(\sigma) - Z(s)} \\ &- \int_{-\infty}^{\infty} \frac{\chi_1(\bar{Z}(\sigma) + \mathrm{i}(\lambda+1))\bar{Z}'(\sigma)\,\mathrm{d}\sigma}{\bar{Z}(\sigma) - Z(s)}\,, \end{aligned}$$

where $Z(\sigma) = z(\sigma) - \mathrm{i}(\lambda+1)$ and $\bar{Z}$ denotes complex conjugate of Z. Note that the first integral in the above equation is singular in the Cauchy principal value sense as $\sigma \to s$. Taking the imaginary part of this equation then gives

$$\begin{aligned} \pi[x'(s)\phi_1'(s) - \gamma] = &\int_{-\infty}^{\infty} \frac{(\phi_1'(\sigma) - \gamma x'(\sigma))(y(s) - y(\sigma)) - \gamma y'(\sigma)(x(\sigma) - x(s))}{(x(\sigma) - x(s))^2 + (y(\sigma) - y(s))^2}\,\mathrm{d}\sigma \\ &- \int_{-\infty}^{\infty} \frac{(\phi_1'(\sigma) - \gamma x'(\sigma))(Y(\sigma) + Y(s)) - \gamma y'(\sigma)(x(\sigma) - x(s))}{(x(\sigma) - x(s))^2 + (Y(\sigma) + Y(s))^2}\,\mathrm{d}\sigma \end{aligned} \tag{2.11}$$

where $Y(s) = y(s) - \lambda - 1$.

A similar method as outlined above is used to derive two integrodifferential equations for the lower layer. The method of images cannot be used in any simple way for this case and so the contour, entirely in the lower layer, consists of the interfacial surface, the bottom surface $y = B(x)$ and the vertical lines $x = \pm L$ with $L \to \infty$. The first of these equations has added to the contour a semicircle of vanishingly small radius centred on the point $z = z(s)$ on the interfacial surface and is given by

$$\oint_\Gamma \frac{\chi_2(z)\,\mathrm{d}z}{z - z(s)} = 0\,,$$

where $\chi_2(z) = \mathrm{d}w_2/\mathrm{d}z - 1$. Taking the imaginary part gives

$$\begin{aligned} \pi[x'(s)\phi_2'(s) - 1] = &\int_{-\infty}^{\infty} \frac{(\phi_2'(\sigma) - x'(\sigma))(y(\sigma) - y(s)) + y'(\sigma)(x(\sigma) - x(s))}{(x(\sigma) - x(s))^2 + (y(\sigma) - y(s))^2}\,\mathrm{d}\sigma \\ &- \int_{-\infty}^{\infty} \frac{B'(x)(x - x(s)) + (B(x) - y(s))(u_2(x)(1 + B'(x)^2) - 1)}{(x - x(s))^2 + (B(x) - y(s))^2}\,\mathrm{d}x\,. \end{aligned} \tag{2.12}$$

The second of the two equations in the lower layer has added to the contour a semicircle of vanishingly small radius excluding the point $z = z^* = x^* + \mathrm{i}B(x^*)$ on the bottom surface and is given by

$$\pi[u_2(x^*) - 1] = \int_{-\infty}^{\infty} \frac{(\phi_2'(\sigma) - x'(\sigma))(y(\sigma) - B(x^*)) + y'(\sigma)(x(\sigma) - x^*)}{(x(\sigma) - x^*)^2 + (y(\sigma) - B(x^*))^2} \, d\sigma$$
$$- \int_{-\infty}^{\infty} \frac{B'(x)(x - x^*) + (B(x) - B(x^*))(u_2(x)(1 + B'(x)^2) - 1)}{(x - x^*)^2 + (B(x) - B(x^*))^2} \, dx . \quad (2.13)$$

Note in equation (2.12) the first integral has a Cauchy principal value singularity at $\sigma = s$ and in equation (2.13) the second integral has a Cauchy principal value singularity at $x = x^*$.

To find the surface $y = S(x)$, we need to solve the three coupled integrodifferential equations (2.11)–(2.13) subject to the Bernoulli equation (2.9), the arclength condition (2.8) and the upstream asymptotic conditions (2.7).

Once this surface is known, we may compute other quantities of interest, as will be shown in Section 4. For example a measure of the energy lost as the fluid flows over the obstacle is given by the nondimensional drag G, where

$$G = \int_{-L}^{L} p_2 B'(x) \, dx .$$

Here we have assumed that the obstacle is in the interval $-L \leq x \leq L$ and p_2 is the pressure evaluated on the bottom $y = B(x)$. Using the Bernoulli equation on the bottom surface, this is written more conveniently as

$$G = \frac{-F_2^2}{2} \int_{-L}^{L} u_2^2(1 + B'(x)^2)B'(x) \, dx . \quad (2.14)$$

3. The linearised solution

An approximate solution to the equations of motion may be derived for the case when the dimensionless mountain height h is a small quantity. We then express the interface and velocity potentials as the regular perturbations

$$S(x) = 1 + hS_1(x) + O(h^2) \quad (3.1)$$

$$\phi_1(x, y) = \gamma x + h\phi_{11}(x, y) + O(h^2) \quad (3.2)$$

$$\phi_2(x, y) = x + h\phi_{21}(x, y) + O(h^2) . \quad (3.3)$$

Here $S_1(x)$, $\phi_{11}(x, y)$ and $\phi_{21}(x, y)$ are to be determined, and for a symmetric mountain profile given by

$$B(x) = hf(x) = h \int_0^{\infty} M(k) \cos kx \, dk \quad (3.4)$$

where $M(k)$ determines the mountain profile, may be shown to have the forms

$$S_1(x) = \int_0^{\infty} a(k) \cos kx \, dk \quad (3.5)$$

$$\phi_{11}(x, y) = \int_0^\infty b(k) \cosh[k(y - 1 - \lambda)] \sin kx \, dk \tag{3.6}$$

$$\phi_{21}(x, y) = \int_0^\infty (c(k) \cosh[k(y - 1)] + d(k) \sinh[k(y - 1)]) \sin kx \, dk \, . \tag{3.7}$$

The linearised forms of the conditions (2.3)–(2.6) then yield

$$a(k) = \frac{F_2^2 k M(k) \sinh k\lambda}{E(k)} \, ,$$

where

$$E(k) = (F_2^2 k \cosh k - (1 - D) \sinh k) \sinh k\lambda + \gamma^2 D F_2^2 k \sinh k \cosh k\lambda \, , \tag{3.8}$$

with similar expressions for $b(k)$, $c(k)$ and $d(k)$. The dispersion relation for the linearised problem is given by $E(k_0) = 0$, where k_0 is the wavenumber of the downstream waves. In this paper, we consider the smooth mountain profile

$$f(x) = \begin{cases} \frac{1}{2}(1 + \cos \pi x/L) & -L \leqslant x \leqslant L \\ 0 & \text{otherwise} \, . \end{cases} \tag{3.9}$$

This profile was chosen for its ease of use with Fourier transforms for the linear theory and in this case gives

$$a(k) = \frac{\pi F_2^2 \sin kL \sinh k\lambda}{L^2(\pi^2/L^2 - k^2)E(k)} \, .$$

The linearised solution (3.5)–(3.7) possesses a wave train in the lee of the mountain only when the dispersion relation has a nonzero real solution, that is when

$$\frac{F_2^2(\gamma^2 D + \lambda)}{\lambda(1 - D)} < 1 \, . \tag{3.10}$$

It is convenient to express equation (3.5) as the difference between two integrals in the form

$$S_1(x) = \frac{\pi F_2^2}{4L^2} \left[\int_{-\infty}^{\infty} \frac{\sin[k(x + L)] \sinh k\lambda}{(\pi^2/L^2 - k^2)E(k)} \, dk - \int_{-\infty}^{\infty} \frac{\sin[k(x - L)] \sinh k\lambda}{(\pi^2/L^2 - k^2)E(k)} \, dk \right] . \tag{3.11}$$

Each integral in equation (3.11) has the same form, which is convenient for calculation purposes, but is singular with poles on the real axis at $k = \pm k_0$. In order to obtain an interface profile with an oscillatory nature downstream of the obstacle, but no waves upstream, we interpret the integral as the Cauchy principal value with the addition of the contributions by integrating around the singularities along a semicircular path of vanishingly small radius passing below the singularities at $k = \pm k_0$. In the case when the fluid depths far upstream in each layer are equal ($\lambda = 1$) the dispersion relation shows that the wavelength associated with $S_1(x)$ downstream of the obstacle will remain constant in the linear theory if $F_2^2(\gamma^2 D + 1)/(1 - D)$ is a constant.

The linearised wave drag is calculated by substituting equations (3.3) and (3.7) into the nonlinear expression (2.14). We obtain

$$G = \frac{F_2^2 h^2 \pi^4 T(k_0) \sin^2 k_0 L}{L^4 (\pi^2/L^2 - k_0^2)^2 E'(k_0)} \tag{3.12}$$

where

$$T(k) = \sinh k\lambda[(D-1)\cosh k + F_2^2 k \sinh k] + \gamma^2 D k F_2^2 \cosh k\lambda \sinh k$$

and the terms $O(h^3)$ have been ignored.

4. Numerical method

In this section we present the numerical method used to solve approximately the system of equations (2.7)–(2.9) and (2.11)–(2.13). We will solve for the interfacial boundary at N equally spaced points $s_1, s_2, \ldots, s_N$ with the points s_1 and s_N representing $-\infty$ and ∞, respectively. This numerical method is similar to that used by Forbes and Schwartz [5] and Forbes [14], and need not be described in great detail here.

In order to discretise the integrodifferential equations it is also necessary to choose grid points on the bottom $y = B(x)$. Here we choose to take densely spaced points over the region where the mountain profile changes more rapidly with x. For example, in the case of the profile given by equation (3.9) this region of more densely spaced points will be $-L \leqslant x \leqslant L$. On the bottom we therefore take M points, $x_1, x_2, \ldots, x_M$ not necessarily equally spaced, again with the points x_1 and x_M approximating $-\infty$ and ∞, respectively.

The singularities in each of the integrodifferential equations are subtracted and the singular integrals are thus replaced by non-singular integrals plus logarithmic terms. The integrodifferential equations are evaluated at $N-1$ midpoints given by, $s_{j+1/2} = \frac{1}{2}(s_j + s_{j+1})$, $j = 1, \ldots, N-1$ in the case of those solving for quantities on the interface and at the $M-1$ midpoints given by, $x_{j+1/2} = \frac{1}{2}(x_j + x_{j+1})$, $j = 1, \ldots, M-1$ for the equation solving for the horizontal velocity component on the bottom surface. Once the vector of values $y'(s_j)$, $j = 1, \ldots, N$ is known, the remainder of the variables in the problem may be calculated. Newton's method is used to solve for these quantities as follows:

1. Make a guess at $y'(s_2), \ldots, y'(s_N)$, noting we take $y'(s_1) = 0$ to satisfy the condition of uniform flow at upstream infinity. The initial guess may be a vector of zeros, the corresponding $y'(s_j)$ values calculated from the linear solution or the $y'(s_j)$ calculated from a previous non-linear solution.
2. Integrate $y'(s_j)$ numerically to get $y(s_j)$, $j = 2, \ldots, N$ using the upstream condition $y(-\infty) \approx y(s_1) = 1$.
3. Calculate $x'(s_j)$, $j = 2, \ldots, N$ using equation (2.8) and integrate as in (2) using the upstream condition $x(s_1) = s_1$.
4. Solve the discretised version of equation (2.11) to find $\phi_1'(s_j)$. We also need the condition $\phi_1'(s_1) = \gamma$ to give as many equations as unknowns.
5. Calculate $\phi_2'(s_j)$ using the Bernoulli equation (2.9) on the surface.
6. Calculate $u_2(x_j)$ on the bottom surface using the discretised version of equation (2.13). At this stage all the variables are known.

7. We use the remaining integrodifferential equation (2.12) as a cost function, update the values of $y'(s_j)$, and return to (2).

The iterations are terminated when some norm of the cost function is sufficiently close to zero. At this stage all the quantities of interest on the boundaries are known. Since the velocity potential in each layer is harmonic, we can now determine any other quantities at any point in either layer through the use of Cauchy's integral formula (and possibly the Bernoulli equation, for example to calculate the pressure at some point in either layer).

5. Numerical results

When the above scheme was implemented on the computer it was found, in most cases, to converge in only a few iterations. Indeed, for mountains of height $h = 0.001$ the solution took only two iterations and was found to trace the linear solution almost exactly for most parameter values, confirming the accuracy of our method for small disturbances. It was also found that in the case when the fluid depths far upstream in each layer were equal ($\lambda = 1$), the non-linear solution had waves with constant wavelength if the remaining parameters were varied in such a way that the ratio $F_2^2(\gamma^2 D + 1)/(1 - D)$ remained constant. This behaviour repeated that observed in the linear theory.

As the mountain height is increased the nonlinear nature of the problem starts to take effect. Figure 2 shows a comparison of linear and non-linear results for the case when the depths far upstream in each layer are equal ($\lambda = 1$), the fluid speeds far upstream in each layer are equal ($\gamma = 1$), the density ratio of the layers is $D = 0.7$, and the Froude number in the lower layer is $F_2 = 0.2$. The mountain profile is that given by equation (3.4) with $h = 0.301$ and $f(x)$ given by equation (3.9) with $L = 0.5$. The amplitude of the non-linear waves is far greater than that for the linear waves and also we note the compression of the wavelength for this large mountain. This is consistent with the results presented by Forbes and Schwartz [5].

Figure 3 shows how the effect of increasing the mountain height is to increase the influence

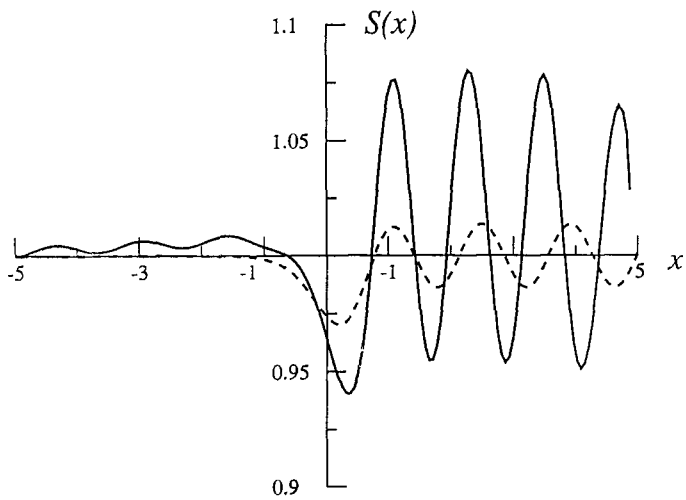

Fig. 2. A comparison of wave profiles for the case $\lambda = 1$, $\gamma = 1$, $F_2 = 0.2$, $D = 0.7$, $L = 0.5$ and $h = 0.301$. The non-linear profile (solid line) differs greatly from the linear profile (dashed line) for this large mountain.

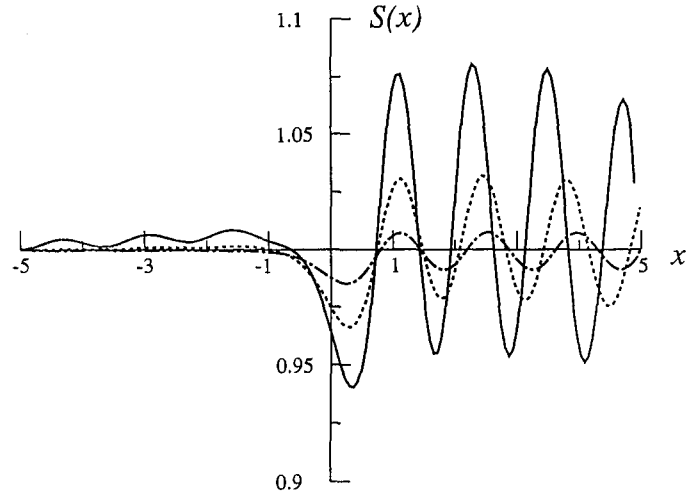

Fig. 3. Non-linear wave profiles at various mountain heights for the case $\lambda = 1$, $\gamma = 1$, $F_2 = 0.2$, $D = 0.7$ and $L = 0.5$. The mountain heights are $h = 0.101$ (chain line), $h = 0.201$ (dashed line), and $h = 0.301$ (solid line).

of non-linearity on the problem. The amplitude of the waves increases in a non-linear manner and the wavelength is compressed further as the mountain height increases.

In both Figs 2 and 3 we notice some inconsistencies in the last half wavelength downstream and also the occurence of upstream waves ahead of the obstacle. This is due to the fact that when the problem is solved numerically the interval over which we obtain a solution has to be truncated from an infinite length to that of six to eight wavelengths. The reader is again referred to Forbes and Schwartz [5] where the effects of truncating the problem at either end of the interval are explained in greater depth.

Any non-linearity in a problem such as this can be illustrated by comparing the linear and non-linear drag as the height of the obstacle is increased. Our expression for non-linear drag (2.14) was found to agree with its linear counterpart (3.12) for small obstacles, and the non-linear results continued to be reliable even for mountains of moderate height. However, as the obstacle height was increased, we found the evaluation of the integral in equation (2.14) to become increasingly sensitive to numerical error, caused by worsening loss of significance errors. Instead we discuss the variation of downstream wave amplitude with obstacle height. Figure 4 shows how the peak to trough amplitude A of the waves varies with the obstacle height h, for two different obstacle lengths, $L = 0.5$ and $L = 0.75$, with the remaining parameter values as mentioned above. The circles represent the amplitude of the $L = 0.5$ solutions and the squares represent the amplitude of the $L = 0.75$ solutions. For comparison purposes, we have also plotted the lines indicating how the amplitude of the waves generated by the linear solution varies with mountain height, the black line representing the $L = 0.5$ solutions and the grey line the $L = 0.75$ solutions. Again the divergence of the linear and non-linear results for large h clearly highlights the non-linear nature of the problem. For these parameter values the method failed to produce waves greater than those for a mountain of height $h = 0.326$ when the mountain had half length $L = 0.5$ or a mountain of height $h = 0.321$ when $L = 0.75$.

This figure prompts two important questions. Firstly, for mountains of half length $L = 0.5$ we notice that the amplitude of the downstream waves near mountains of height $h = 0.120$ appears to be higher than we might expect. This behaviour is also noted near mountains of

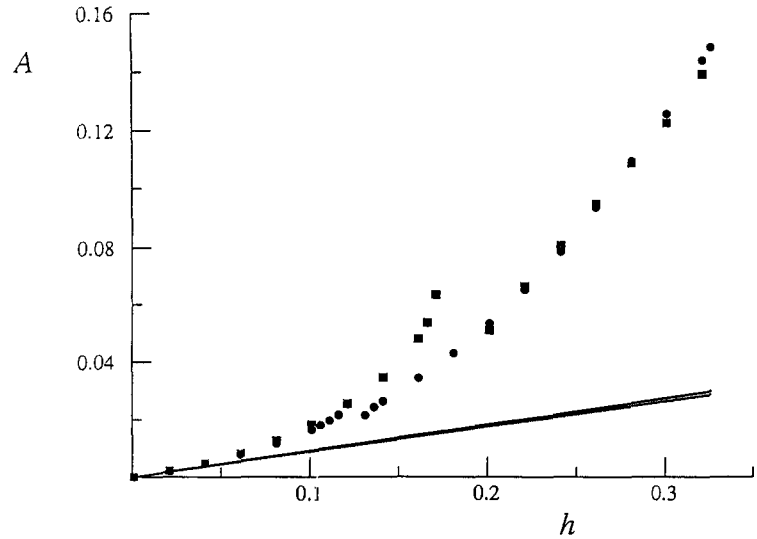

Fig. 4. A comparison of the downstream wave amplitude produced by the non-linear theory (dots) and the linear theory (lines) as the mountain height is increased for two different mountain lengths when $\lambda = 1$, $\gamma = 1$, $F_2 = 0.2$ and $D = 0.7$. The black line and black dots represent results for $L = 0.5$ while the grey line and grey dots represent results for $L = 0.75$. The numerical method was unable to produce reliable results for mountains with heights between $h = 0.121$ and $h = 0.131$ when $L = 0.5$ and mountain heights between $h = 0.171$ and $h = 0.201$ when $L = 0.75$.

height $h = 0.170$ when $L = 0.75$. The first question is then, why does the amplitude of the downstream waves vary in this way? To answer this question we need to consider the work by Forbes [4] in which drag free flows over an ellipse were investigated. It was found in the non-linear theory that for any given ellipse height, there exist an infinite number of ellipse lengths, behind which there are no downstream waves. This result was not entirely unexpected as Lamb [15] showed this behaviour in the linearised theory. The linear theory presented in this paper in Section 3 for the mountain profile given by equation (3.9) also predicts such behaviour as well as predicting obstacle lengths for which the downstream waves will have a relative maximum in amplitude. Forbes found that as the height of the obstacle was increased in his non-linear theory, so the obstacle length had to be increased to obtain the relevant wave free solution (see Fig. 3 in Forbes [4]). Thus, we expect that, to obtain waves of a relative maximum in amplitude as we increase the mountain height, we must also increase the obstacle length. On the other hand, if we increase the obstacle height without increasing the obstacle length, we can expect to move through heights where we are crossing curves on the obstacle height versus obstacle length plane on which we either have wave free solutions or solutions with a relative maximum in amplitude. Thus, the curves in Fig. 4 cannot in general be expected to rise monotonically, but instead may possess local maxima and minima. Now, in Fig. 4, we are using constant mountain lengths of $L = 0.5$ and $L = 0.75$. With the parameters as given above the linear theory predicts a relative maximum in amplitude for an obstacle length of $L \approx 0.356$. This set of solutions with a relative maximum in amplitude obviously passes through the points $L = 0.5$ at an obstacle height of $h \approx 0.120$ and $L = 0.75$ at an obstacle height of $h \approx 0.170$ where in Fig. 4, the amplitude of the waves is larger than we might otherwise expect from the solutions obtained for mountain heights near these values.

The second question Fig. 4 poses is why do the waves reach some sort of maximum height, in other words, why does the method fail to compute waves higher than those for $h = 0.326$ when $L = 0.5$ and $h = 0.321$ when $L = 0.75$? We especially need to consider this question in the light of work by Holyer [13], Grimshaw and Pullin [11] and Turner and Vanden-Broeck [12] who each investigated limiting interfacial gravity waves. In these works solutions were sought for waves without regard for their mechanism of generation and as such could be investigated over an interval of a single wavelength. In our calculations we have had to include an interval of six to eight wavelengths over the obstacle, so here the numerical grid is much too coarse to obtain the accuracy one can gain by considering a single wavelength. The maximum amplitude solutions we obtain resemble more closely those obtained by Holyer [13] where the limiting wave was expected to have vertical tangents in its profile, rather than those in Grimshaw and Pullin [11] where the limiting profile was subsequently shown to be mushroom–shaped. Turner and Vanden-Broeck [12] found solutions to oscillate between waves with a vertical section and waves with an overhang. We also note that the limiting solutions presented in the latter two of the three papers above are not the maximum amplitude solutions but are arrive at in a different manner than in steps of increasing amplitude. Given our method of calculating the wave profiles and our inability to use large numbers of points, it is not surprising to find our wave profiles falling short of those generated in the papers above.

Figure 5 shows the effect of varying the ratio of fluid velocities γ in each layer. Before further comments are made, we note that equation (2.11) is invariant under the transformation $\gamma \to -\gamma$ and $\phi_1'(s) \to -\phi_1'(s)$. In other words, reversing the direction of fluid flow in the top layer does not change the shape of the interface. Presumably, however, the solutions obtained in the reverse flow case would be unstable in a time dependent model.

It is clear from Fig. 5 that both the amplitude and wavelength of the waves decreases as the upstream velocity ratio is decreased. From equation (3.8) we can see that as the value of γ is decreased the value of k_0 will increase; thus the linear solution predicts the behaviour observed in Fig. 5.

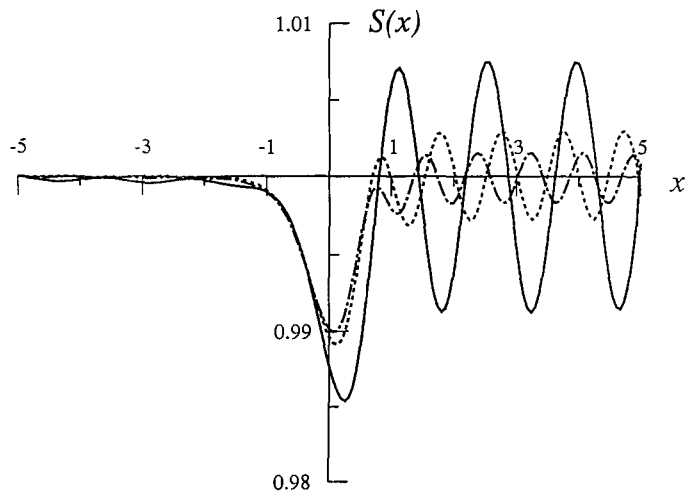

Fig. 5. Non-linear wave profiles at different values of the ratio of upstream fluid speeds γ, for the case $\lambda = 1$, $F_2 = 0.2$, $D = 0.7$, $L = 0.5$ and $h = 0.1$. The profiles are for $\gamma = 0$ (chain line), $\gamma = 0.5$ (dashed line) and $\gamma = 1$ (solid line).

6. Summary and discussion

A method of solution has been presented for calculating the two-dimensional flow over an arbitrary topography of a two layer system of fluid. This arises in looking for a simple model for atmospheric waves in the lee of a mountain.

The linearised solution in Section 3 yielded the important relationship (3.10) involving the parameters F_2, γ, λ and D, that enabled us to predict when downstream waves were likely to occur.

A fully non-linear solution was developed using a boundary integral approach, which when discretised, gave us a set of three systems to solve. This set of equations was solved iteratively using Newton's method, and the interface was found to consist of a wave free region upstream of the obstacle, followed by a periodic wave downstream of the obstacle. A check on our results was provided by comparing the results for the linear and non-linear theories, which were found to be in very good agreement for small mountains. The non-linearity became evident, however, as the obstacle height was increased and the non-linear interface developed waves of an amplitude far in excess of the amplitude of the waves of the linear interface. Our method was successful in calculating waves with a nearly vertical tangent to them as in Holyer [13], and it is unreasonable to expect overhanging waves as described in work by Grimshaw and Pullin [11] and Turner and Vanden-Broeck [12] due to the relatively few points per wavelength we were able to employ. We note that such waves may be unstable even if the steady equations predicted them.

As noted in the Introduction, Shen [10] has considered a similar two layer model for flow over an obstacle using a forced Korteweg-de Vries equation. He however allows the upper layer to be bounded above by a free surface, rather than the rigid lid used in the current work. This difference in formulation makes comparison of the results obtained from this forced Korteweg-de Vries theory with the results obtained from the fully non-linear theory impossible, without reworking the asymptotic results using the different boundary condition. We have therefore been unable to compare our results meaningfully with asymptotic theories, although a comparison of the forced Korteweg-de Vries theory of Shen [10] with the non-linear theory used here is currently under investigation for single layer flows. These results will be published elsewhere.

The boundary integral technique used here is very versatile in that it can be used to solve for the flow over an arbitrarily shaped obstacle. At present we are in the process of using this approach on a different model for the atmosphere where the upper layer is now regarded as compressible as proposed in Forbes and Belward [16]. In addition critical flow problems are being investigated with this method, as in Forbes [14]. Such solutions are of importance in the study of severe downslope winds in meteorology.

Acknowledgement

This work was supported by an Australian Postgraduate Research Award.

References

1. W. Kelvin, On stationary waves in flowing water, *Phil. Mag.* 22 (1886) 353–357.
2. J.V. Wehausen and E.V. Laitone, Surface waves, *Handbuch der Physik*, vol. 9, Springer, 1960.

3. L.K. Forbes, On the wave resistance of a submerged semi-elliptical body, *J. Eng. Math.* 15 (1981) 287–298.
4. L.K. Forbes, Non-linear, drag-free flow over a submerged semi-elliptical body, *J. Eng. Math.* 16 (1982) 171–180.
5. L.K. Forbes, and L.W. Schwartz, Free-surface flow over a semicircular obstruction, *J. Fluid Mech.* 114 (1982) 299–314.
6. F. Dias, and J.-M. Vanden-Broeck. Open channel flows with submerged obstructions, *J. Fluid Mech.* 206 (1989) 155–170.
7. A.C. King, and M.I.G. Bloor, Free surface flow of a stream obstructed by an arbitrary bed topography, *Quart. J. Mech. Appl. Math.* 43 (1990) 87–106.
8. R.H.J. Grimshaw and N. Smyth, Resonant flow of a stratified fluid over topography, *J. Fluid Mech.* 169 (1986) 429–464.
9. S.S.P. Shen, Disturbed critical surface waves in a channel of arbitrary cross section, *Z. Angew. Math. Phys.* 40 (1989) 216–229.
10. S.S.P. Shen, Forced solitary waves and hydraulic falls in two-layer flows, *J. Fluid Mech.* 234 (1992) 583–612.
11. R.H.J. Grimshaw and D.I. Pullin, Extreme interfacial waves, *Phys. Fluids* 29 (1986) 2802–2807.
12. R.E.L. Turner, and J.-M. Vanden-Broeck, The limiting configuration of interfacial gravity waves, *Phys. Fluids* 29 (1986) 372–375.
13. J.Y. Holyer, Large amplitude progressive interfacial waves, *J. Fluid Mech.* 93 (1979) 433–448.
14. L.K. Forbes, Two-layer critical flow over a semi-circular obstruction, *J. Eng. Math.* 23 (1989) 325–342.
15. H. Lamb, Hydrodynamics, 6th edn., Cambridge University Press, 1932.
16. L.K. Forbes and S.R. Belward, Atmospheric interfacial waves, *Phys. Fluids A* 4 (1992) 2222–2229.